Dalton Transactions

An international journal of inorganic chemistry

Accepted Manuscript

ROYAL SOCIETY OF CHEMISTRY

rsc.li/dalton

View Article Online
DOI: 10.1039/D6DT00824K

Strain-Specific Synergy: An Oxo-Rhenium(V) Complex Potentiates Antibiotic Efficacy in *Staphylococcus aureus* strains

Gozde Demirci[a], Youri Cortat[a], Aurélien Crochet[a], Emanuele Calia[b], Simon G. Sprecher[b], Fabio Zobi[a,*]

[a]Department of Chemistry, University of Fribourg, Chem. du Musée 9, 1700 Fribourg, Switzerland

[b]Department of Biology, University of Fribourg, Chem. du Musée 10, 1700 Fribourg, Switzerland

*Correspondence: fabio.zobi@unifr.ch

Keywords: oxo-rhenium(V), antibacterial activity, MRSA, ampicillin, efflux pump inhibition

Abstract

In this study, a library of oxo-rhenium(V) complexes of general formula [$Cl_3ReO(NN)$] bearing diimine ligands was synthesized and fully characterized. The complexes were evaluated for antibacterial activity against Gram-positive and Gram-negative bacteria (MSSA, MRSA, *E. coli*, and *P. aeruginosa*). Increasing the lipophilicity of the diimine ligand led to an enhancement in biological activity. The most active compound, bearing NN = bathocuproine (complex **9**), exhibited potent activity against *S. aureus* strains (MIC = 2 µM). Its toxicity profile was assessed *in vitro* and *in vivo*: cytotoxicity toward L929 fibroblasts afforded a therapeutic index (TI) of 4.9, while evaluation in the invertebrate model *Artemia salina* showed only 12.9% lethality at 4× MIC after 24 h, indicating a favorable preliminary safety profile. Mechanistic investigations in MSSA and MRSA revealed strain-specific synergistic interactions of **9** with chloramphenicol and tetracycline in MSSA, and with ampicillin in MRSA, increasing the therapeutic index up to 19.5. Notably, co-administration of sub-inhibitory concentrations of ampicillin and **9** suppressed MRSA growth for more than 72 h. Computational studies suggest that complex **9** may interfere with the β-lactam resistance pathway in MRSA.

Introduction

The rapid emergence of antimicrobial resistance (AMR) represents one of the most pressing challenges in modern medicine. In particular, infections caused by methicillin-resistant *Staphylococcus aureus* (MRSA) remain difficult to treat and are associated with significant morbidity and mortality.[1] The declining effectiveness of conventional antibiotics has therefore

View Article Online
DOI: 10.1039/D6DT00824K

stimulated the search for alternative therapeutic strategies capable of overcoming bacterial resistance mechanisms. In this context, metal-based compounds have attracted renewed attention as potential antimicrobial agents because their structural diversity, tunable coordination environments, and redox properties can enable mechanisms of action that differ fundamentally from those of purely organic antibiotics.[2-6]

Among the different metal ions explored in medicinal inorganic chemistry,[7-12] complexes of ruthenium,[13-20] gold,[21-24] and rhenium[25-31] have shown particular promise. Ruthenium complexes, for example, have been extensively investigated for their anticancer and antimicrobial properties, demonstrating how their chemical and structural versatility can be exploited to design biologically active coordination compounds.[32, 33] Rhenium has also emerged as attractive element for the development of bioactive metal complexes.[34] Most studies in rhenium bioinorganic chemistry have focused on tricarbonyl complexes of the general type *fac*-$[Re(I)(CO)_3]^+$. Owing to their well-defined photophysical and photochemical properties, these compounds have been widely investigated for applications in bioimaging, luminescent probes, radiopharmaceuticals, and catalysis.[35-40] In contrast, rhenium complexes in other oxidation states have received significantly less attention in biological studies. In particular, oxo-rhenium(V) and trioxo-rhenium(VII) complexes coordinated by diimine ligands such as 2,2'-bipyridine and 1,10-phenanthroline derivatives have been reported,[41-43] yet their potential in biological applications remains comparatively underexplored.

Building upon our broader interest in antimicrobial rhenium species, we have began to explore oxo-Re(V) complexes.[44-46] From a coordination chemistry perspective, oxo-rhenium(V) complexes offer a robust and versatile structural core. The Re=O core typically adopts a distorted octahedral geometry in which the terminal oxo ligand exerts a strong *trans* influence, while the remaining coordination sites can accommodate a variety of mono- or bidentate ligands. This structural arrangement provides a stable yet chemically tunable framework that allows systematic modification of the ligand sphere without disrupting the integrity of the metal-oxo core. Diimine ligands such as bipyridine and phenanthroline derivatives enable fine control over electronic properties, steric environment, and lipophilicity, parameters that are often critical in determining the biological activity and cellular uptake of metal compounds.[8, 34]

View Article Online
DOI: 10.1039/D6DT00824K

Previous studies focused on antimicrobial applications[47-49] have demonstrated that oxo-Re(V) complexes may display activity against clinically relevant pathogens such as *S. aureus* and *Candida albicans*.[50] More recently, the research group of Patra reported detailed investigations into the anticancer activity of oxo-Re(V) complexes together with mechanistic insights into their mode of action.[51, 52] Despite these advances, systematic studies exploring the relationship between ligand design, physicochemical properties, and antibacterial activity in oxo-rhenium(V) complexes remain limited.

In the present work, we address this gap by synthesizing and characterizing a library of oxo-Re(V) complexes of general formula [$Cl_3ReO(NN)$] bearing diimine (NN) ligands with systematically varied lipophilicity. The compounds were evaluated for their antibacterial activity against Gram-positive and Gram-negative bacteria and a relationship between ligand lipophilicity and antibacterial activity against Gram-positive strains, including MSSA and MRSA, was observed. Among the investigated compounds, complex **9**, bearing NN = bathocuproine, exhibited the highest activity, with a minimum inhibitory concentration (MIC) of 2 µM against *S. aureus* strains and a therapeutic index of 4.9. Notably, complex **9** showed synergistic activity with ampicillin in MRSA at very low antibiotic concentrations. The biocompatibility of this compound was further evaluated through cytotoxicity studies in L929 fibroblasts and an *in vivo* toxicity model using *Artemia salina*. In the latter assay, complex **9** showed only 12.9% lethality at 8 µM (4× MIC) after 24 h incubation, indicating relatively low acute toxicity.

Results and Discussion

Synthesis and characterization

The series of oxo-rhenium(V) complexes of the general formula [$Cl_3ReO(NN)$] was synthesized using ten different diimine ligands as outlined in Figure 1. Although related oxo-rhenium(V) complexes have been previously reported,[43, 53] the incorporation of structurally diverse rigid diimine ligands in this series enables a systematic investigation of their structural and spectroscopic properties. The formation of the oxo-rhenium(V) core was confirmed by standard spectroscopic techniques and X-ray driffraction. All complexes displayed a characteristic ν(Re=O) stretching band in the range 966-989 cm^{-1} (ESI), consistent with

View Article Online
DOI: 10.1039/D6DT00824K

literature values for terminal oxo ligands in Re(V) systems. Minor variations in the stretching frequency across the series likely reflect differences in the electronic properties of the coordinated diimine ligands. Electronic absorption spectra of the complexes exhibited broad bands in the 400-500 nm region (ESI), which can be attributed to metal-to-ligand charge transfer (MLCT) transitions involving the rhenium center and the π* orbitals of the diimine ligands. The position and intensity of these bands showed modest dependence on ligand structure, in line with the expected modulation of ligand π-acceptor properties.

View Article Online
DOI: 10.1039/D6DT00824K

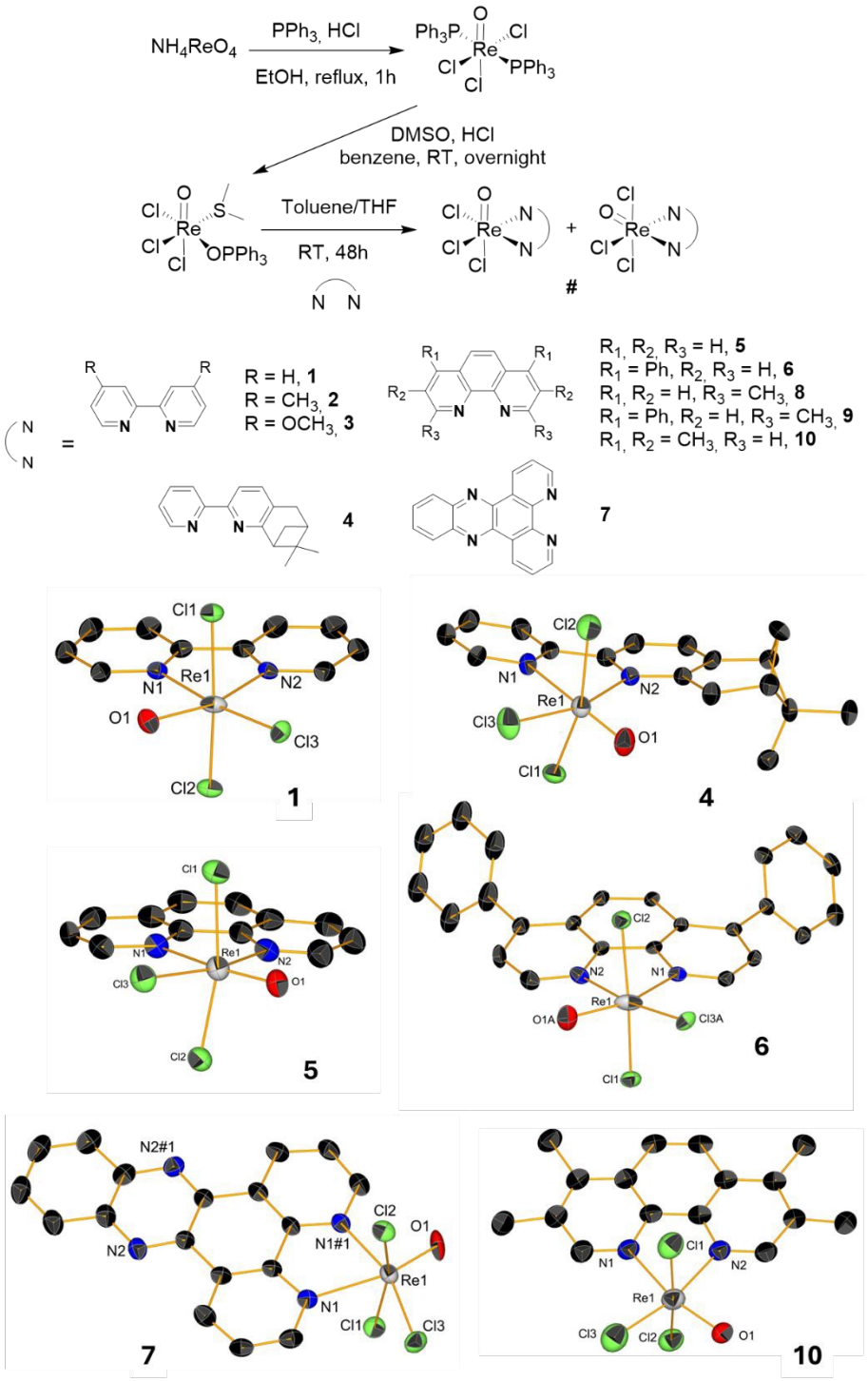

Figure 1. Top: synthetic scheme of $[Cl_3ReO(NN)]$ species. Bottom: crystal structure of complexes **1**, **4**-**7** and and **10**. Thermal ellipsoids are at 30% probability. Hydrogen atoms are omitted for clarity.

View Article Online
DOI: 10.1039/D6DT00824K

The solution structures of the complexes were investigated by ^{1}H NMR spectroscopy. For several isolated derivatives (**2**, **3**, **5**, and **7**), two distinct sets of proton resonances were observed (ESI), indicating the coexistence of two geometric isomers in solution. This behavior is attributed to the presence of the equatorial-O (*mer* isomer) and the axial-O (*fac* isomer) configurations within the distorted octahedral coordination sphere. For instance, the isolated complexes **2** and **3** predominantly exhibit the *mer* configuration in solution (ca. 79% and 67%, respectively), while complexes **5** and **7** favor the *fac* configuration (93% and 89%, respectively). Conversely, the isolated complexes **1**, **4**, and **6** display a single set of resonances corresponding exclusively to the *mer* isomer, whereas the phenanthroline-type complexes (**8–10**) are observed solely as the *fac* isomer in solution (see ESI). This solution behavior stands in contrast to our solid-state observations. Single-crystal X-ray diffraction analysis of the complexes revealed exclusively the *mer* isomer (Figure 1).

To gain deeper insight into this apparent discrepancy, density functional theory (DFT) calculations were performed at the PBE0-D3BJ/def2-SVP (SMD, solvent = THF) level of theory. The computational results reveal that the thermodynamic energy differences (ΔG) between the two configurations are remarkably small, typically spanning a range of only 1 to 2.5 kcal/mol (ESI). For complexes **1**, **5**, **7**, and the phenanthroline series (**8–10**), the *mer* isomer is calculated to be the most stable species in solution by ca. 1 to 2 kcal/mol. For **4**, the two isomers are virtually isoenergetic, while for **3** and **6**, the *fac* isomer is predicted to be slightly more stable by ca. 1 to 2 kcal/mol. The mismatch between the computationally predicted solution stabilities, the NMR integration ratios, and the solid-state structures suggests that the isolation of these complexes is governed by a combination of kinetic control and phase-separation thermodynamics (i.e. the relative solubility of the species in the specific reaction conditions). Because the complexes were isolated as solids that precipitate directly from the reaction mixture, the solid-state distribution does not reflect a purely relaxed solution equilibrium. Instead, the exclusive presence of the *mer* isomer in the solid-state structures is likely a consequence of the thermodynamic equilibrium established during the crystallization, and its lower solubility which shifts the solution equilibrium toward the *mer* form via continuous precipitation under the crystallization conditions.

View Article Online
DOI: 10.1039/D6DT00824K

Further characterization was attempted using photoluminescence and electrospray ionization mass spectrometry. However, no photoluminescence was observed for the oxo-Re(V) complexes, consistent with the absence of emissive excited states in this class of compounds. Similarly, no molecular ion peaks corresponding to intact complexes were detected by ESI-MS, likely due to the limited ionization of these species.

Antimicrobial effects

The antibacterial activities of the synthesized complexes were evaluated against MSSA, MRSA, *Escherichia coli*, and *Pseudomonas aeruginosa* strains (Table 1 and ESI). In order to assess selectivity and biocompatibility, the effects of the compounds were examined using L929 mouse fibroblast cells and *Artemia salina* organisms as representative models of normal cells and whole-organism toxicity, respectively. Complexes containing the bipyridine-type ligands (**1**-**4**) did not show measurable antibacterial activity, suggesting that this ligand type is not conducive to antimicrobial efficacy within this series. Conversely, complexes **6, 8, 9**, and **10** demonstrated significant antibacterial activity against the Gram-positive strains, with relative MIC values roughly correlating to their lipophilicity (Figure 2A). However, the therapeutic indices of **6, 8,** and **10** were below 1 (Table 1), implying limited selectivity due to pronounced toxicity toward normal cells. It is noteworthy that complex **9** exhibited a considerably higher therapeutic index (4.9) against Gram-positive bacteria, indicating a favorable balance between antibacterial potency and biocompatibility. However, the complexes showed no activity against Gram-negative bacteria, a finding that is likely attributable to the inherent permeability barrier imposed by the outer membrane of these strains. Collectively, our results identified complex **9** as the most promising antibacterial candidate in this series, with selective activity against Gram-positive pathogens and an acceptable safety profile.

Entry [a]	MIC (μM)				IC_{50} (L929) (μM)
	MSSA	**MRSA**	***E. coli***	***P. aeruginosa***	

View Article Online
DOI: 10.1039/D6DT00824K

a	>128	>128	>128	>128	>15
b	>128	>128	>128	>128	>15
1	>128	>128	>128	>128	>15
2	>128	>128	>128	>128	>15
3	>128	>128	>128	>128	>15
4	>128	>128	>128	>128	10.01 ± 2.4
5	128	128	64	>128	7.01 ± 1.4
6	16 (TI:0.4)	16 (TI:0.4)	>128	>128	5.75 ± 2.2
7	>128	>128	>128	>128	>15
8	32 (TI:0.5)	64 (TI:0.2)	64	>128	>15
9	2 (TI:4.9)	2 (TI:4.9)	64	>128	9.76 ± 2.9
10	16 (TI:0.1)	16 (TI:0.1)	64	>128	1.65 ± 0.5
***Artemia salina* lethality assay**					
	Control	**6 (8× MIC)**	**9 (1× MIC)**	**9 (2× MIC)**	**9 (4× MIC)**
Mortality	2.9 ± 0.3 %	13.7 ± 0.9 %	4.8 ± 0.4 %	4.8 ± 0.4 %	12.9 ± 1.0 %

Table 1. Top part: MIC values of the complexes in bacterial strains, and the IC_{50} value in L929 (μM) cells after 24 hours. MIC: Minimal inhibition concentration, IC_{50}: 50% viability concentration, TI: Therapeutic index (IC_{50}(L929) / MIC(strain)). Bottom part: *Artemia salina* lethality assay after 24 hours.

[a] **a** and **b** are the rhenium precursor complexes $Re(O)Cl_3(PPh)_2$ and $Re(O)Cl_3(SMe_2)(OPPh_3)$ respectively. The activity of ligands was investigated previously. See reference 28.

To further evaluate the toxicity of complex **9**, its effects were assessed using the *Artemia salina* lethality assay as a measure of general biocompatibility (Table 1, Figure 2B). *Artemia salina*, a species of brine shrimp, is widely used as a rapid and cost-effective *in vivo* screening model for assessing the toxicity and safety profile of bioactive compounds, and has been shown to correlate well with toxicity in higher organisms.[54, 55] Compound **9** exhibited a mortality rate of only 12.9% at a concentration corresponding to 4× MIC (8 μM) in *Artemia salina*, indicating a low level of acute toxicity even at supra-inhibitory doses. For comparison, the structurally related inactive control complex **6**, with NN = bathophenanthroline, exhibited a mortality rate that was comparable to **9** (13.7%) but at a substantially higher concentration (128 μM). These results suggest that the antibacterial efficacy of complex **9** is not accompanied by proportional

View Article Online
DOI: 10.1039/D6DT00824K

toxicity and that its activity against MRSA is likely due to specific antibacterial mechanisms rather than nonspecific cytotoxic effects.

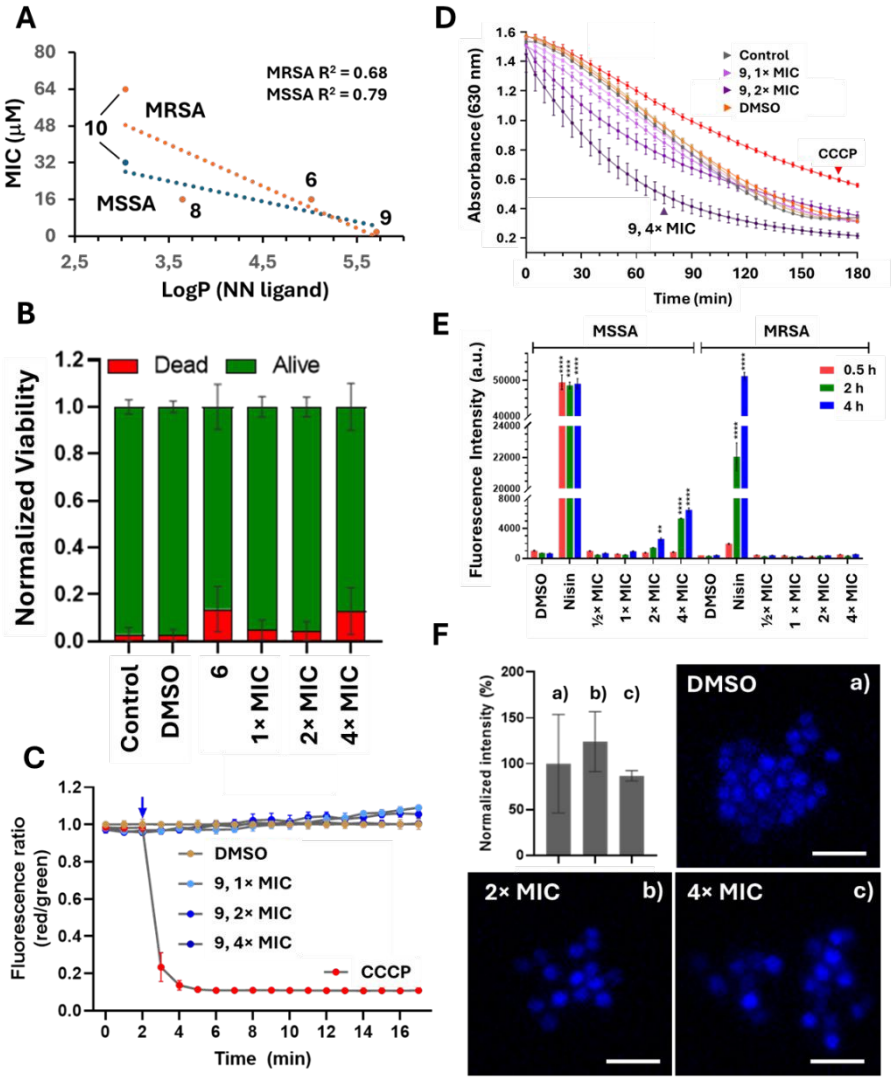

Figure 2. Antibacterial activity, toxicity, and mechanistic evaluation of complex **9**. **A**. Correlation between lipophilicity and antibacterial activity of complexes **6**-**10** against Gram-positive strains, showing decreasing MIC values with increasing lipophilicity. **B**. Toxicity assessment in *Artemia salina* after 24 h exposure to DMSO (1%), complex **6** (128 μM), and complex **9** at 1×, 2×, and 4× MIC. Data represent the normalized % viability of *Artemia salina* nauplii as a mean values from six independent replicates, with standard deviations indicated. **C**. Effect of complex **9** on bacterial membrane potential in *S. aureus* strains, assessed using the $DiOC_2(3)$ probe and expressed as the red/green fluorescence ratio over time. No significant changes were observed compared to the negative control (DMSO), while CCCP (25 μM, 2× MIC) was used as a positive control. **D**. Resazurin reduction assay evaluating the impact of complex **9** on bacterial metabolic activity. No inhibitory effect on respiration was observed; instead, an increased rate of resazurin reduction was detected in MRSA at 4× MIC. **E**. Membrane integrity assessment by propidium iodide (PI) uptake assay. Fluorescence intensity was measured after 0.5, 2, and 4 h incubation. Increased PI uptake was observed in MSSA after 4 h at 2× MIC, whereas no significant membrane permeabilization was detected in MRSA

View Article Online
DOI: 10.1039/D6DT00824K

under the same conditions. **F**. Effect of complex **9** on cell wall synthesis probed by HADA incorporation after 15 min exposure. Scale bar: 5 µm. Quantification of fluorescence intensity (bar graph, 500 cells per experiment, three independent replicates) is shown alongside representative fluorescence microscopy images of *S. aureus* cells treated with 2× and 4× MIC of **9** compared to the DMSO control.

Since most active antimicrobial Re complexes appear to act either on the bacterial membrane or the cell wall synthesis,[29, 56, 57] we next performed experiments to evaluate the effect of complex **9** on the membranes of Gram-positive strains (Figure 2). This study employed PI and $DiOC_2(3)$ probes, respectively. $DiOC_2(3)$ (3,3'-diethyloxacarbocyanine iodide) was used to assess the effect of complex **9** on bacterial membrane potential. This green fluorescent dye forms red fluorescent aggregates as membrane potential increases.[58] Experiments performed on MSSA and MRSA strains revealed no detectable effect of the complex **9** on membrane potential, as the results were comparable to those of the negative control (Figure 2C).

As no effect on bacterial membrane potential was observed in the $DiOC_2(3)$ assay, we next investigated whether the compound impacts cellular metabolic activity using a resazurin reduction assay (Figure 2D). Resazurin is a redox-sensitive dye that is reduced by metabolically active cells to the fluorescent compound resorufin, and is therefore widely used as an indicator of cellular respiration and viability.[59] CCCP (100 µM) and sodium azide (NaN_3, 15 mM) were employed as positive controls; however, sodium azide is not an optimal respiratory inhibitor for *S. aureus* because this organism lacks a classical cytochrome c oxidase and relies on alternative terminal oxidases that are less sensitive to azide inhibition.[60] Complex **9** did not exhibit a notable inhibitory effect on bacterial respiration (Figure 2D). Instead, in the MRSA strain, **9** induced a marked increase in the rate of resazurin reduction, particularly evident at a concentration equivalent to 4× MIC. These results suggest that **9** accelerated the metabolic activity of MRSA at high concentrations, reflecting a possible induced stress response in *S. aureus* that transiently enhanced cellular redox activity.

Given that no alterations in intracellular redox activity were detected, we next assessed whether the compound affects bacterial membrane integrity using the propidium iodide (PI) uptake assay. In cases of severe membrane damage, the membrane-impermeable PI dye can penetrate the cell and intercalate into DNA.[61] PI red fluorescence intensity was measured after incubation periods of 0.5, 2, and 4 hours. A significant increase in red fluorescence was

View Article Online
DOI: 10.1039/D6DT00824K

observed after 4 hours of incubation with 2× MIC of complex **9** in MSSA. In contrast, no PI uptake was detected in MRSA, even after 4 hours of incubation (Figure 2E). Finally, we probed whether **9** may exert it antibacterial action by interfering with the peptidoglycan biosynthesis. To visualize the bacterial cell wall under fluorescence microscopy, the fluorescent D-amino acid probe HADA (7-hydroxycoumarin-3-carboxylic acid–D-alanine) was employed. HADA is metabolically incorporated into the peptidoglycan of actively growing bacteria *via* the cell wall biosynthesis machinery, enabling its direct visualization.[62] In the HADA staining experiment performed on MSSA, no significant changes in HADA fluorescence intensity were observed compared to the control (Figure 2F), indicating that interrupting the cell wall synthesis is unlikely to contribute to the mechanism of action of **9**.

As **9** did not show measurable effects in the aforementioned assays, we sought to gain further insight into its potential mechanism of action by examining its interactions with established antibiotics using checkerboard assays. Prior to this, we evaluated whether the inactive and non-toxic complexes **1, 2, 3, 4,** and **7**, could potentiate the activity of vancomycin against MRSA, as vancomycin remains a clinically relevant first-line treatment for MRSA infections and thus provides a suitable reference for assessing potential synergistic or sensitizing effects. For the co-injection experiments, the complexes (5 µM) were administered simultaneously with varying concentrations of vancomycin and bacteria incubated for 48 hours (Figure 3A and ESI). After 24 hours, a reduction of approximately 40% in bacterial growth was observed, particularly in the presence of complexes **1** and **2**. For complexes **3, 4,** and **7**, a reduction in bacterial growth was also detected under complex-only conditions, suggesting a mild growth-modulating effect independent of vancomycin. To assess whether pre-exposure to these complexes could sensitize bacteria to vancomycin, sequential addition experiments were performed (Figure 3B), in which vancomycin was added 24 hours after treatment with the complexes (5 µM). Under these conditions, no significant inhibition of bacterial growth was observed, even at 1×, 2×, or 4× MIC concentrations of vancomycin (1.25, 2.5, and 5 µg/mL, respectively). The results indicate that, although certain non-active complexes modestly suppress bacterial growth when co-administered, they do not induce sustained physiological changes that enhance susceptibility to vancomycin.

View Article Online
DOI: 10.1039/D6DT00824K

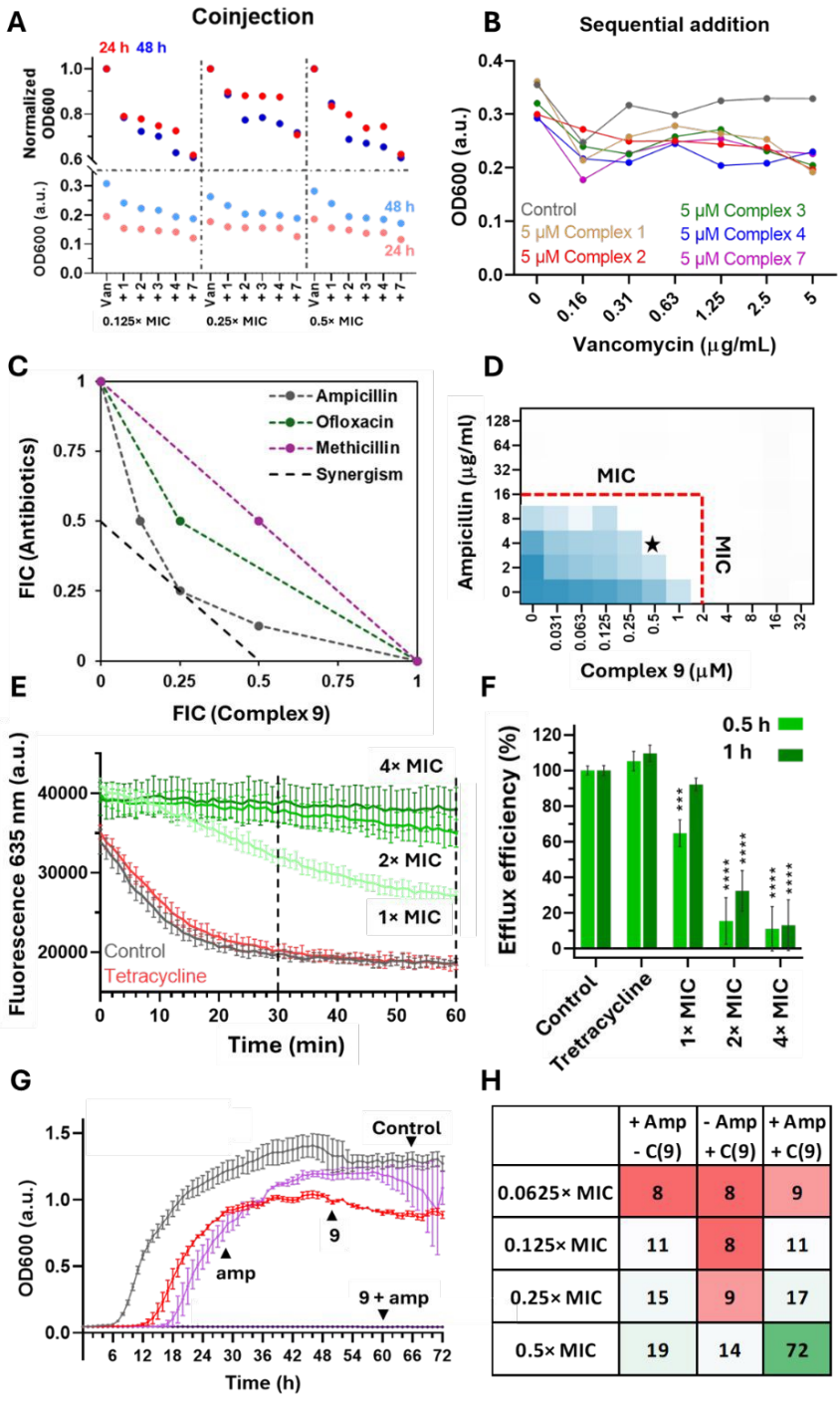

Figure 3. Evaluation of the combinatorial antibacterial effects and mechanistic investigations of [$Cl_3ReO(NN)$] complexes. **A**. Bacterial viability of *S. aureus* in the presence of increasing concentrations of vancomycin and 5 µM of complexes **1**-**4** and **7** after 24 h and 48 h incubation. Optical density (OD_{600}) values (light colors) and normalized OD_{600} values (dark colors) relative to the corresponding vancomycin concentrations are shown. **B**. Sequential treatment assay in MRSA with complexes **1**-**4** and **7**. Cells were pre-treated with 5 µM complexes for 24 h, followed by addition of vancomycin at varying concentrations. Bacterial growth and viability was assessed after a further 24 h by measuring OD_{600} of the samples. **C**. Fractional inhibitory concentration (FIC) plots illustrating synergistic interactions of complex **9** with ampicillin in

View Article Online
DOI: 10.1039/D6DT00824K

MRSA. **D**. MRSA checkerboard heat map assays of complex **9** in combination with ampicillin after 24 h incubation. **E**. Efflux pump activity assessed by ethidium bromide (EtBr) accumulation assay in MRSA strains. Fluorescence intensity (λ = 635 nm) was monitored over time following treatment with complex **9** at 1×, 2×, and 4× MIC, compared to control and tetracycline. **F**. Quantification of MRSA efflux efficiency in the presence of increasing concentrations of complex **9** at 0.5 and 1h post treatment. Statistical significance is indicated by asterisks (*** P < 0.0002, **** P < 0.0001). **G**. Time-kill kinetics showing MRSA bacterial growth over 72 h upon treatment with complex **9**, ampicillin, and their combination (0.5× MIC). **H**. Heat map representation of bacterial growth inhibition across combinations of different concentrations ampicillin and complex **9**, highlighting sustained suppression of MRSA growth for at least 72 h at sub-inhibitory concentrations (0.5× MIC ampicillin and **9**).

Checkerboard assays evaluating the combined effects of complex **9** with various antibiotics were then performed against MSSA and MRSA strains (ESI). The results of these assays revealed synergistic interactions between complex **9** and chloramphenicol as well as tetracycline in the MSSA strain, while a synergistic effect was observed with ampicillin in the MRSA strain (Figure 3C and D). The significant synergy observed between complex **9** and tetracycline lead us to the hypothesis that **9** could inhibit bacterial efflux pumps. To this end we performed the ethidium bromide (EtBr) efflux assay with both MSSA (ESI) and MRSA strains (Figure 3E and F). In the MSSA strain, complex **9** induced a moderate and constitent inhibition of EtBr efflux (approximately 30–40%), that remained unaffected by both concentration and incubation time, indicating a partial or nonspecific interference with efflux activity. Conversely, a substantially more pronounced and concentration-dependent efflux inhibition was observed in the MRSA strain, where approximately 65% inhibition was achieved within 30 minutes at 1× MIC and surpassed 90% inhibition at 4× MIC (Figure 3E and F). Tetracycline resistance in *S. aureus* is predominantly mediated by efflux pumps, such as Tet(K), Tet(L), and multidrug transporters, including NorA.[63] Inhibition of these systems would be expected to increase intracellular tetracycline accumulation, and restore antibiotic susceptibility. The enhanced efflux inhibition observed in MRSA is consistent with the significant synergism between complex **9** and tetracycline, thereby supporting the hypothesis that complex **9** functions, at least in part, as an efflux pump inhibitor.

The synergistic interaction between complex **9** and ampicillin was further validated using time-dependent bacterial growth assays against the MRSA strain (Figure 3G and H). Co-administration of sub-inhibitory concentrations of ampicillin (0.0625× MIC, 0.5 μg/mL) and complex **9** (0.5× MIC, 1 μM) resulted in a pronounced delay in bacterial growth, extending the

View Article Online
DOI: 10.1039/D6DT00824K

lag phase by approximately 15 hours compared to treatment with ampicillin alone. Notably, complete suppression of bacterial growth was achieved for up to a minimum of 72 hours when ampicillin at 0.5× MIC (4 μg/mL) was combined with 0.5× MIC (1 μM) of complex **9**, indicating a strong and sustained synergistic effect.

MRSA resistance to β-lactam antibiotics arises from two distinct but coordinated mechanisms in response to the antibiotic challenge (Figure 4).[64] After detection of the antibiotic, the BlaR1 receptor promotes expression of the low-affinity penicillin-binding protein PBP2a (encoded by the *mecA* gene) and the β-lactamase enzyme PC1 (encoded by the *BlaZ* gene).[65] The latter hydrolyzes the β-lactam ring of susceptible antibiotics such as ampicillin and penicillin, rendering them inactive. In contrast, methicillin is resistant to β-lactamase-mediated hydrolysis and its lack of efficacy against MRSA is attributed to its poor inhibition of PBP2a.[66] The observed potentiation of ampicillin activity suggests that complex **9** may interfere with this resistance mechanism. Thus, we decided to employ molecular docking studies to explore potential interactions of complex **9** with PBP2a and related targets involved in cell wall biosynthesis and antibiotic resistance. The docking analysis revealed that complex **9** exhibits favorable binding affinities toward these key MRSA resistance-associated proteins, with calculated binding energies of -9.0 kcal/mol for BlaR1, -8.6 kcal/mol for PC1, and -9.8 kcal/mol for PBP2a (Figure 4), indicating that multiple components of the β-lactam resistance machinery may be targeted.

However, when considered together with the biological data, a strain-dependent mechanism emerges for the complex. In MSSA, complex **9** does not potentiate β-lactam antibiotics but instead shows synergism with tetracycline and chloramphenicol. This behavior, supported by ethidium bromide efflux assays (ESI), indicates that **9** acts primarily as an efflux pump inhibitor in this strain. In contrast, in MRSA, complex **9** induces a markedly stronger and concentration-dependent inhibition of efflux, reaching over 90% inhibition at 4× MIC (Figure 3E). While this effect likely contributes to increased intracellular antibiotic concentration, it does not fully account for the highly selective synergism observed with ampicillin. Since **9** does not show synergism with methicillin, this suggests that inhibition of the β-lactamase system (i.e. PC1 in Figure 4), rather than direct targeting of PBP2a, plays a central role. Thus, in this context, the interaction of **9** with PC1, and its possible Inhibition, would reduce enzymatic degradation of

View Article Online
DOI: 10.1039/D6DT00824K

ampicillin providing a mechanism for restoring antibiotic susceptibility. Overall, our data support a dual and strain-dependent mode of action for complex **9**. In MSSA, its activity is dominated by moderate efflux pump inhibition, whereas in MRSA, strong efflux inhibition is complemented by interference with the β-lactamase resistance pathway. Among the possible targets, PC1 appears to us as the most functionally relevant in explaining the selective potentiation of ampicillin, while PBP2a binding, although energetically favorable *in silico*, is unlikely to represent the primary mechanism of action.

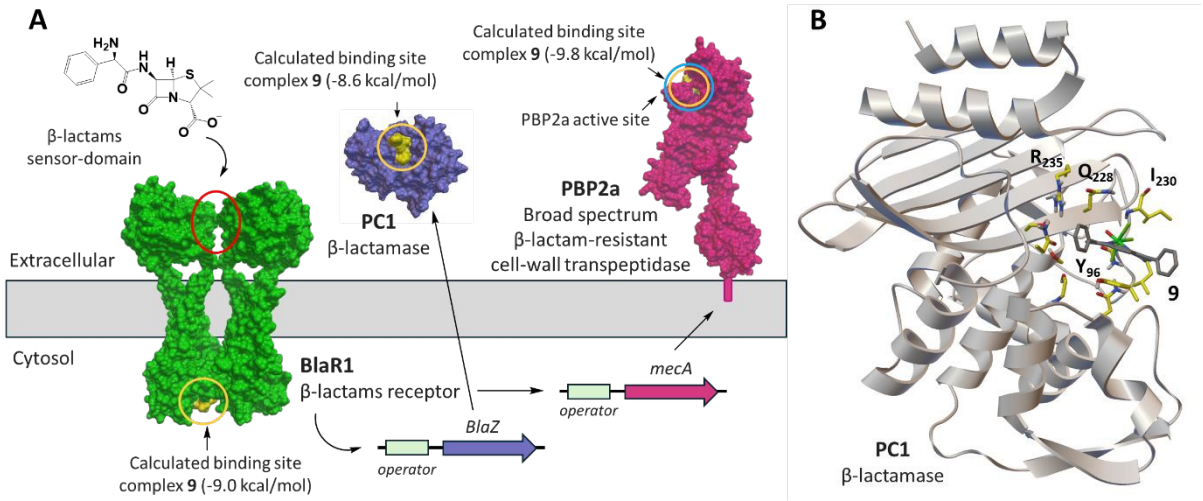

Figure 4. A. Schematic representation of the MRSA mechanism of resistance to β-lactam antibiotics. Depicted are the BlaR1 (β-lactam receptor, PDB:8EXP),[67] the PC1 β-lactamase (PDB:6WGR), and PBP2a (PDB:4DKI)[68] showing the calculated lowest energy binding sites and docking values of **9**. The complex was predicted to bind BlaR1 at its cytosolic domain (-9.0 kcal/mol), PC1 near the active site (-8.6 kcal/mol), and PBP2a at the transpeptidase (TP) active site (-9.8 kcal/mol). **B**. Structural model of the interaction of **9** with PC1, highlighting in yellow some flexible amino acids residues in the binding region of the complex.

Conclusion

In this work, a series of oxo-Re(V) complexes of general formula [$Cl_3ReO(NN)$] was synthesized and systematically investigated to elucidate structure-activity relationships governing their antibacterial properties. Modulation of the diimine ligand lipophilicity was found to play a key role in tuning biological activity, with the bathocuproine-containing complex **9** emerging as the most active derivative. Complex **9** exhibited potent and selective activity against Gram-positive bacteria, including MRSA (MIC = 2 μM), while remaining inactive toward Gram-negative strains. The compound displayed a favorable toxicity profile, combining low *in vivo*

View Article Online
DOI: 10.1039/D6DT00824K

toxicity in the *Artemia salina* model with good cytocompatibility toward L929 fibroblasts. Mechanistic studies indicated that complex **9** does not significantly affect membrane potential or overall respiratory activity. Instead, it induces alterations in intracellular redox processes under stress conditions and, notably, strongly inhibits efflux pump activity, particularly in MRSA (>90% inhibition at 4× MIC). These findings provide a mechanistic basis for the pronounced, strain-dependent synergistic effects observed with clinically relevant antibiotics. In particular, complex **9** significantly potentiated β-lactam activity in MRSA, leading to sustained growth suppression for at least 72 h at sub-inhibitory concentrations. Molecular docking studies further support a multi-target mode of action, revealing favorable interactions with key proteins involved in β-lactam resistance (PBP2a, BlaR1, and BlaZ), consistent with interference in the resistance pathway. In contrast, structurally related but inactive complexes did not exhibit synergistic behavior, pointing to the important role of ligand design in dictating biological function. Overall, these results demonstrate that fine-tuning of the coordination sphere in oxo-Re(V) complexes enables control over their biological activity and highlights complex **9** as a promising scaffold for the development of metal-based antibacterial agents and antibiotic adjuvants targeting Gram-positive resistance mechanisms.

Materials and Methods

All chemicals were used in high purity. Infrared (IR) measurements were performed with a Bruker TENSOR II with the following parameters: 16 scans for the background and 32 scans for the sample with a resolution of 4 cm^{-1} in the 4000 to 600 cm^{-1} region. UV-Vis analysis of the complexes was measured on a Jasco V730 spectrophotometer. Nuclear magnetic resonance (NMR) measurements were obtained with a Bruker Advance III 400 MHz instrument. Cytotoxicity and antimicrobial tests were validated by using Tecan-Infinity M Nano with iControl program and Tecan-Spark 10M with SparkControl program respectively. 96-well plates were purchased from Sarstedt. The antimicrobial activity of complexes was assessed against *Staphylococcus aureus* 113 (methicillin sensitive, MSSA), *Staphylococcus aureus* mecA R2954 (methicillin resistant, MRSA), *Escherichia coli* (25922) and *Pseudomonas aeruginosa* (MPAO1 WT)[69] strains. L929 mouse fibroblast cell line were kindly gifted from Prof. David Hoogewijs, Department of Medicine, University of Fribourg, Switzerland. Microscope images were collected with a Leica DM6B widefield fluorescence microscope with 63× oil

View Article Online
DOI: 10.1039/D6DT00824K

magnification in the Bioimaging Core Facilities, University of Fribourg, Switzerland. Microscope images were analyzed and quantified by using the LAS X and ImageJ programs. 1× and 2× Mueller-Hinton Broth (MHB) medium obtained from BioLife was prepared according to producer instructions. For cation-adjusted MHB (CAMHB) medium, 0.04 mg/mL Ca^{2+} and 0.02 mg/mL Mg^{2+} were added by using $CaCl_2$ and $MgSO_4$ salt respectively. 0.9% NaCl solution was prepared and autoclaved before use. 7-hydroxycoumarincarbonylamino-d-alanine (HADA) was prepared according to a published procedure.[70] Dulbecco's Modified Eagle Medium (DMEM) (with L-glutamine and glucose), penicillin/streptomycin with L-glutamine (pen/strep with l-glu) and trypsin-EDTA were purchased from Pan, Biotech. Thiazolyl blue tetrazolium bromide (MTT) was provided by Thermoscientific – Acros. Fetal bovine serum (FBS) and phosphate buffered saline (PBS, 1×) solution was obtained from Gibco. The computational docking analysis was performed as previously descrived.[44] Single-crystal X-ray diffraction data for the compounds were acquired using a Stoe STADIVARI diffractometer equipped with $CuK\alpha_1$ radiation (λ = 1.5406 Å) and an Oxford Cryosystems cryostat. The structures were determined by intrinsic phasing with the SHELXT program and subsequently refined by least-squares minimization using SHELXL. All crystallographic data generated in this study have been deposited with the Cambridge Crystallographic Data Centre (CCDC). The supplementary crystallographic information is available under CCDC deposition numbers 2539772-2539777.

Synthesis methods

The rhenium precursor complexes $Re(O)Cl_3(PPh)_2$ (**a**) and $Re(O)Cl_3(SMe_2)(OPPh_3)$ (**b**) were synthesized according to literature procedures with modified reaction times.[43, 71] Specifically, complex **b** was synthesized in 18 hours instead of 5 days. Dipyrido[3,2-a:2',3'-c] phenazine was synthesized according to literature.[72, 73]

General procedure for synthesis of the complexes

Complex **b** (typically 0.1 mmol, 65 mg) and the corresponding ligand (1:1.2 molar ratio) were dissolved in the indicated solvent (5-10 mL) and stirred for 24-48 h. The resulting products were isolated by filtration and washed with appropriate solvents (THF and/or toluene). For

View Article Online
DOI: 10.1039/D6DT00824K

complexes **8**-**10**, the ligand was used in a 1:2 molar ratio relative to complex **b**. The reactions were performed in THF (48 h), followed by filtration and washing with THF, toluene, or ethyl acetate.

(1) [$Cl_3ReO(NN)$] where NN = 2,2'-Bipyridine. The complex was previously reported using a different synthesis method.[43, 53] Prepared in THF (24 h). Product isolation and crystallization were performed by slow evaporation from DCM. Yield: 13 mg of green crystals, 28%. IR (solid, cm^{-1}): 979 (Re=O). UV-Vis (DCM, λ_{max} [nm]): 455, 299. ^1H NMR (400 MHz, CD_3CN, ppm): δ = 8.71 (d, J=7.8 Hz, 1 H), 8.64 - 8.67 (m, 1 H), 8.29 - 8.33 (m, 1 H), 8.23 - 8.26 (m, 1 H), 8.17 - 8.22 (m, 1 H), 7.91 (ddd, J=7.5, 6.0, 1.3 Hz, 1 H), 7.68 - 7.74 (m, 1 H), 7.42 (ddd, J=7.5, 5.7, 1.2 Hz, 1 H).

(2) [$Cl_3ReO(NN)$] where NN = 4,4'-Dimethyl-2,2'-bipyridine. The complex was previously reported.[43] Yield: 32 mg, 65%. IR (solid, cm^{-1}): 979 (Re=O). UV-Vis (DCM, λ_{max} [nm]): 448, 293. ^1H NMR (400 MHz, CD_3CN, ppm): δ = 8.53 (d, J=0.9 Hz, 1 H), 8.47 (d, J=6.0 Hz, 1 H), 8.15 (d, J=0.7 Hz, 1 H), 8.06 (d, J=6.0 Hz, 1 H), 7.72 (d, J=7.2 Hz, 1 H), 7.23 - 7.26 (m, 1 H), 3.35 (s, 3 H), 2.49 (s, 3 H).

(3) [$Cl_3ReO(NN)$] where NN = 4,4'-Dimethoxy-2,2'-bipyridine. Prepared in THF (48 h). Yield: 51 mg, 97.3%, yellow powder. IR (solid, cm^{-1}): 977 (Re=O). UV-Vis (DCM, λ_{max} [nm]): 441, 266. ^1H NMR (400 MHz, CD_3CN, ppm): δ = 8.59 (d, J=6.4 Hz, 1 H), 8.43 (d, J=6.7 Hz, 1 H), 8.18 (d, J=2.6 Hz, 1 H), 8.09 (d, J=2.8 Hz, 1 H), 8.01 (d, J=6.8 Hz, 1 H), 7.77 (d, J=2.6 Hz, 1 H), 7.41 (dd, J=6.8, 2.7 Hz, 1 H), 7.27 (dd, J=6.4, 2.6 Hz, 1 H), 6.95 (dd, J=6.7, 2.6 Hz, 1 H), 4.21 (s, 3 H), 4.09 (s, 3 H), 4.01 - 4.03 (s, 3 H).

(4) [$Cl_3ReO(NN)$] where NN = 5,6-Pinene-2,2'-bipyridine. Prepared in THF (48 h). Yield: 42 mg, 75%, green powder. IR (solid, cm^{-1}): 987 (Re=O). UV-Vis (DCM, λ_{max} [nm]): 441, 307, 266. ^1H NMR (400 MHz, CD_3CN, ppm): δ = 8.70 (dq, J=5.7, 0.8 Hz, 1 H), 8.41 (d, J=8.2 Hz, 1 H), 8.14 (d, 2 H), 7.40 (ddd, J=7.1, 5.6, 1.8 Hz, 1 H), 7.29 (s, 1 H), 3.85 (dd, J=18.7, 3.2 Hz, 1 H), 3.61 - 3.68 (m, 1 H), 3.03 - 3.07 (m, 1 H), 2.70 - 2.78 (m, 1 H), 2.47 (dq, J=6.1, 3.1 Hz, 1 H), 1.44 (s, 3 H), 1.37 (d, J=10.0 Hz, 1 H), 0.70 (s, 3 H). Crystallization was performed by layering (DCM/pentane).

View Article Online
DOI: 10.1039/D6DT00824K

(5) [$Cl_3ReO(NN)$] where NN = 1,10-Phenanthroline. Previously reported.[53, 74] Prepared in toluene (48 h). Yield: 6 mg, 12.3%, light brown powder. IR (solid, cm^{-1}): 983 (Re=O). UV-Vis (DCM, λ_{max} [nm]): 412, 268. ^1H NMR (400 MHz, CD_3CN, ppm): δ = 9.33 (dd, J=5.0, 1.5 Hz, 2 H), 8.89 (dd, J=8.3, 1.5 Hz, 2 H), 8.23 (s, 2 H), 8.12 (dd, J=8.3, 5.0 Hz, 2 H). Crystallization was performed by layering (DCM/pentane).

(6) [$Cl_3ReO(NN)$] where NN = 4,7-Diphenyl-1,10-phenanthroline. Prepared in THF (48 h). Yield: 49 mg, 78%, yellow powder. IR (solid, cm^{-1}): 982 (Re=O). UV-Vis (DCM, λ_{max} [nm]): 462, 424, 283. ^1H NMR (400 MHz, CD_3CN, ppm): δ = 9.07 (d, J=5.5 Hz, 1 H), 8.51 (d, J=5.7 Hz, 1 H), 8.20 - 8.25 (m, 2 H), 8.07 (d, J=9.5 Hz, 1 H), 7.70 - 7.74 (m, 1 H), 7.61 - 7.68 (m, 10 H). Crystallization was performed by layering (DCM/pentane).

(7) [$Cl_3ReO(NN)$] where NN = Dipyrido[3,2-a:2′,3′-c]phenazine. Prepared in THF (48 h). Yield: 30 mg, 50%, dark powder. IR (solid, cm^{-1}): 979 (Re=O). UV-Vis (DCM, λ_{max} [nm]): 464, 354, 278. ^1H NMR (400 MHz, DMSO-d_6, ppm): δ = 9.73 - 9.78 (m, 2 H), 9.31 (d, J=4.6 Hz, 2 H), 8.44 (dd, J=6.5, 3.4 Hz, 2 H), 8.17 - 8.21 (m, 2 H), 8.11 - 8.15 (m, 2 H). Crystallization was performed by layering (DCM/pentane).

(8) [$Cl_3ReO(NN)$] where NN = Neocuproin. Yield: 21 mg, 40%, pale brown powder. IR (solid, cm^{-1}): 966 (Re=O). UV-Vis (DCM, λ_{max} [nm]): 304, 284. ^1H NMR (400 MHz, CD_3CN, ppm): δ = 8.74 (d, J=8.4 Hz, 2 H), 8.13 (s, 2 H), 7.94 (d, J=8.4 Hz, 2 H), 3.04 (s, 6 H).

(9) [$Cl_3ReO(NN)$] where NN = Bathocuproine. Yield: 16 mg, 24%, green-yellow powder. IR (solid, cm^{-1}): 987 (Re=O). UV-Vis (DCM, λ_{max} [nm]): 360, 293. ^1H NMR (400 MHz, CD_3CN, ppm): δ = 8.01 (s, 2 H), 7.91 (s, 2 H), 7.64 (s, 10 H), 3.10 (s, 6 H). Anal. Calcd for $C_{26}H_{20}Cl_3N_2ORe$: C, 46.67; H, 3.01; N, 4.19. Found: C, 45.02; H, 2.93; N, 4.05.

(10) [$Cl_3ReO(NN)$] where NN = 3,4,7,8-Tetramethyl-1,10-phenanthroline. Yield: 19 mg, 17%, green-yellow powder. IR (solid, cm^{-1}): 976.5 (Re=O). UV-Vis (DCM, λ_{max} [nm]): 352, 279. ^1H NMR (400 MHz, CD_3CN, ppm): δ = 8.98 (s, 2 H), 8.31 (s, 2 H), 2.82 (s, 6 H), 2.62 (s, 6 H). Crystallization was performed by layering (DCM/pentane).

View Article Online
DOI: 10.1039/D6DT00824K

Biochemical studies

The antimicrobial activity of the complexes was tested against two Gram-positive strains (Methicillin-sensitive *Staphylococcus aureus* [113 wt, MSSA] and Methicillin-resistant *Staphylococcus aureus* [mecA R2954, MRSA]) and two Gram-negative strains (*Escherichia coli* [ATCC 25922, *E. coli*] and *Pseudomonas aeruginosa* [MPAO1 WT, *P. aeruginosa*]) by following the Clinical and Laboratory Standards Institute (CLSI) guidelines and the broth microdilution method of Wiegard *et al.*[75, 76] MHB medium was used as the bacterial liquid culture. Briefly, the complexes were dissolved/suspended in DMSO at a concentration of 12.8 mM. Then, 50 µL of 1× MHB medium was added to a 96-well plate. 50 µL of the complexes diluted to a concentration of 0.512 mM with 1× MHB medium were added to the wells with the highest concentrations. Overnight-grown bacteria were diluted to an optical density at 600 nm (OD_{600}) of 0.004 and added to the test wells at a volume of 50 µL. The bacterial strains were then incubated with the complexes for 24 hours at 37 °C. After incubation, the minimum inhibitory concentration (MIC) values were determined by measuring the optical density at 600 nm. The assay was conducted in four replicates. The complexes were dissolved in dimethyl sulfoxide (DMSO), and the volume ratio at the highest concentration was 1%. Membrane potential, membrane integrity, the effect on peptidoglycan synthesis, the checkerboard assay and resazurin reduction experiments investigating the mechanism of action were performed only on complex **9** in MSSA and MRSA strains according to published procedures.[56, 77]

Efflux pump inhibition experiment

For the efflux pump assay, bacterial cultures were treated with ethidium bromide (EtBr). Cultures were grown to an optical density (OD_{600}) of 0.6, then washed with 20 mM potassium phosphate buffer containing 1 mM $MgCl_2$. The bacterial cells were resuspended in the same buffer to a final OD_{600} of 0.2. The suspension was treated with 5 µg/mL EtBr and 10 µM carbonyl cyanide *m*-chlorophenyl hydrazone (CCCP) and incubated for 60 minutes at 20 °C with shaking. After incubation, the cells were centrifuged at 2500 × g for 5 minutes and resuspended in the same phosphate buffer containing 5% glucose. The resuspended culture was then transferred to a black 96-well microplate and treated with 1× MIC tetracycline (1 µg/mL), 100 µM CCCP, and the test complex at 1×, 2×, and 4× MIC concentrations. The

View Article Online
DOI: 10.1039/D6DT00824K

fluorescence of EtBr was measured at an emission wavelength of 635 nm with excitation at 485 nm over a period of 30 minutes.

Time-dependent bacterial growth experiment

A time-dependent bacterial growth assay was conducted over a 72-hour period by monitoring OD_{600}. The experiment was performed using a specific range of antibiotic and complex concentrations. An overnight bacterial culture was adjusted to an OD_{600} of 0.14 and subsequently diluted 200-fold to obtain a final inoculum concentration of approximately 10^6 CFU/mL. Each concentration was tested in triplicate. Following inoculation, the microplate was placed into the plate reader cassette without a lid, and absorbance readings at 600 nm were recorded at hourly intervals for 72 hours. For the time-dependent growth experiments with the inactive complexes, complexes **1, 2, 3, 4,** and **7** were either co-administered with vancomycin or added sequentially to *S. aureus* cultures. Following co-administration, bacterial growth was monitored by measuring OD_{600} at hourly intervals over a 48-hour period.

In vivo* viability assay on *Artemia salina

Artemia salina eggs were placed in a container of artificial seawater, prepared by dissolving 22.7 g of sea salt in 0.5 L of distilled water. The larvae (nauplii) hatched after 48 hours of incubation at room temperature with strong aeration. The toxicity of the complexes on *Artemia salina* was then evaluated according to the reference protocol.[78] Stock solutions of the complexes were prepared in DMSO at a concentration corresponding to 1% (v/v) in the test wells. Twenty nauplii were added to each well of the 96-well plates in 100 µL of 0.9% NaCl solution. DMSO and the complexes were added into the wells in 5 replicates. The test plate was incubated at 25 °C for 24 hours, and the number of surviving nauplii in each well was evaluated under a microscope. The data were normalized according to the following formula:

$$\text{Normalized} = \frac{\text{Number of dead/alive nauplii}}{\text{Number of total nauplii in replica}}$$

***In vitro* cell toxicity experiments**

The cytotoxicity of the complexes was tested on L929 – mouse fibroblast cells. For the cell culture, DMEM medium supplemented with 10% v/v FBS and 1% v/v Pen/strep with L-

View Article Online
DOI: 10.1039/D6DT00824K

glutamine was used. The cytotoxicity of the complexes were tested for 24 hours with MTT cytotoxicity procedure.[79]

Statistical analysis

The results were analyzed with GraphPad Prism 9 by using ordinary one-way ANOVA analysis of variance followed by multiple Dunnett's comparison test. IC_{50} values were evaluated by using nonlinear regression analysis followed by variable slope. $p < 0.05$ was accepted as a statistically significant difference. Statistical significance: (*) $p < 0.03$, (**) $p < 0.02$, (***) $p < 0.0002$, (****) $p < 0.0001$.

Computational Detalis

All Density Functional Theory (DFT) calculations were performed using the Gaussian 16 software package.[80] Geometry optimizations and subsequent frequency calculations were carried out using the PBE0 hybrid functional.[81] To account for non-covalent interactions and long-range dispersion effects, Grimme's atom-pairwise dispersion correction with Becke–Johnson damping (D3BJ) was applied.[82] The split-valence Ahlrichs basis set def2-SVP was employed for all light atoms (C, H, N, O, Cl) as well as for the rhenium (Re) center.[83] For rhenium, the corresponding def2 effective core potential (ECP) was utilized to replace the core electrons and account for scalar relativistic effects. Solvent effects of tetrahydrofuran (THF) were implicitly incorporated during all steps using the Solvation Model based on Density (SMD).[84] The numerical integrations were executed utilizing the UltraFine grid to ensure convergence stability and precision. Frequency calculations were systematically performed at the same level of theory on the optimized geometries to confirm the nature of the stationary points (ensuring zero imaginary frequencies for ground-state minima).

Author contributions

Gozde Demirci synthesized and characterized all complexes, performed all biological experiments and wrote the original draft; Youri Cortat synthesized the HADA label; Aurélien Crochet performed XRD measurements and analysis; Emanuele Calia, helped with the *in vivo* experiments under the supervision of Simon G. Sprecher; Fabio Zobi supervised the project,

View Article Online
DOI: 10.1039/D6DT00824K

performed *in silico* calculations, and corrected the original draft. All authors have read and approved the manuscript.

Conflicts of interest

There are no conflicts to declare.

Data availability

The data supporting this article have been included as part of the Electronic Supplementary Information (ESI). Crystallographic data for the compounds have been deposited at the Cambridge Crystallographic Data Centre (CCDC) under deposition numbers 2539772-2539777. Copies of the data can be obtained free of charge via the CCDC website. Additional data supporting the findings of this study are available from the corresponding author upon request.

View Article Online
DOI: 10.1039/D6DT00824K

References

1. W.H.O., https://www.who.int/news/item/30-04-2014-who-s-first-global-report-on-antibiotic-resistance-reveals-serious-worldwide-threat-to-public-health, (accessed 2026).
2. Evans A., Kavanagh K.A., *J. Med. Microbiol.,* 2021, **70**, 001363, DOI: 10.1099/jmm.0.001363.
3. Vitali V., Zineddu S., Messori L., *RSC Adv.,* 2025, **15**, 748-53, DOI: 10.1039/d4ra07449a.
4. Das B., Sathyanarayan S., Gupta P., *Dalton Trans.,* 2025, **54**, 10178-206, DOI: 10.1039/d5dt00678c.
5. Montilla F., Carrasco C.J., Galindo A., *Dalton Trans.,* 2025, **54**, 6778-84, DOI: 10.1039/d5dt00400d.
6. Liu Q., Liu L., Yin L., Guo J., Liao X., Li J.*, et al.*, *Dalton Trans.,* 2025, **54**, 17025-59, DOI: 10.1039/d5dt01963j.
7. Cabral Campello M.P., Palma E., Correia I., Paulo P.M.R., Matos A., Rino J.*, et al.*, *Dalton Trans.,* 2019, **48**, 4611-24, DOI: 10.1039/c9dt00640k.
8. Fernandez M., Varela J., Correia I., Birriel E., Castiglioni J., Moreno V.*, et al.*, *Dalton Trans.,* 2013, **42**, 11900-11, DOI: 10.1039/c3dt50512j.
9. Lin Y., Scalese G., Bulman C.A., Vinck R., Blacque O., Paulino M.*, et al.*, *ACS Infect. Dis.,* 2024, **10**, 938-50, DOI: 10.1021/acsinfecdis.3c00577.
10. Rivas F., Medeiros A., Quiroga C., Benitez D., Comini M., Rodriguez-Arce E.*, et al.*, *Dalton Trans.,* 2021, **50**, 1651-65, DOI: 10.1039/d0dt03963b.
11. Frei A., Zuegg J., Elliott A.G., Baker M., Braese S., Brown C.*, et al.*, *Chem. Sci.,* 2020, **11**, 2627-39, DOI: 10.1039/c9sc06460e.
12. Scaccaglia M., Birbaumer M.P., Pinelli S., Pelosi G., Frei A., *Chem. Sci.,* 2024, **15**, 3907-19, DOI: 10.1039/d3sc05326a.
13. Martins P.H.R., Romo A.I.B., Gouveia F.S., Jr., Paz I.A., Nascimento N.R.F., Andrade A.L.*, et al.*, *Dalton Trans.,* 2024, **53**, 12627-40, DOI: 10.1039/d4dt01033g.
14. Wang P., Huang H.Y., Dou L.X., Deng W., Wang J.T., Liao X.W.*, et al.*, *Dalton Trans.,* 2023, **52**, 8737-46, DOI: 10.1039/d3dt00889d.
15. Zhang Q., Xiong Y., Cheng J., Tan Y., Liao X., Wang J., *Dalton Trans.,* 2022, **51**, 1099-111, DOI: 10.1039/d1dt02692e.
16. Liao X., Liu L., Tan Y., Jiang G., Fang H., Xiong Y.*, et al.*, *Dalton Trans.,* 2021, **50**, 5607-16, DOI: 10.1039/d0dt04258g.
17. Demoro B., Rossi M., Caruso F., Liebowitz D., Olea-Azar C., Kemmerling U.*, et al.*, *Biol. Trace Elem. Res.,* 2013, **153**, 371-81, DOI: 10.1007/s12011-013-9653-4.
18. Smitten K., Southam H.M., Fairbanks S., Graf A., Chauvet A., Thomas J.A., *Chemistry,* 2023, **29**, e202203555, DOI: 10.1002/chem.202203555.
19. Smitten K.L., Southam H.M., de la Serna J.B., Gill M.R., Jarman P.J., Smythe C.G.W.*, et al.*, *ACS Nano,* 2019, **13**, 5133-46, DOI: 10.1021/acsnano.8b08440.
20. Smitten K.L., Thick E.J., Southam H.M., Bernardino de la Serna J., Foster S.J., Thomas J.A., *Chem. Sci.,* 2020, **11**, 8828-38, DOI: 10.1039/d0sc03410j.
21. Glisic B.D., Djuran M.I., *Dalton Trans.,* 2014, **43**, 5950-69, DOI: 10.1039/c4dt00022f.
22. Mazzei L., Massai L., Cianci M., Messori L., Ciurli S., *Dalton Trans.,* 2021, **50**, 14444-52, DOI: 10.1039/d1dt02488d.
23. Gascon E., Otal I., Maisanaba S., Llana-Ruiz-Cabello M., Valero E., Repetto G.*, et al.*, *Dalton Trans.,* 2022, **51**, 13657-74, DOI: 10.1039/d2dt01963a.

24. Stevanovic N.L., Kljun J., Aleksic I., Bogojevic S.S., Milivojevic D., Veselinovic A., *et al.*, *Dalton Trans.,* 2022, **51**, 5322-34, DOI: 10.1039/d2dt00411a.
25. Romao C.C., Mendes S.S., Rebelo C., Carvalho S.M., Saraiva L.M., *Dalton Trans.,* 2024, **53**, 11009-20, DOI: 10.1039/d4dt00978a.
26. Siegmund D., Lorenz N., Gothe Y., Spies C., Geissler B., Prochnow P., *et al.*, *Dalton Trans.,* 2017, **46**, 15269-79, DOI: 10.1039/c7dt02874a.
27. Sovari S.N., Vojnovic S., Bogojevic S.S., Crochet A., Pavic A., Nikodinovic-Runic J., *et al.*, *Eur. J. Med. Chem.,* 2020, **205**, 112533, DOI: 10.1016/j.ejmech.2020.112533.
28. Sovari S.N., Radakovic N., Roch P., Crochet A., Pavic A., Zobi F., *Eur. J. Med. Chem.,* 2021, **226**, 113858, DOI: 10.1016/j.ejmech.2021.113858.
29. Fulgencio S., Scaccaglia M., Frei A., *ChemBioChem,* 2024, **25**, e202400435, DOI: 10.1002/cbic.202400435.
30. Horner J., Demirci G., Crochet A., Pavic A., Steiner O.M., Zobi F., *Molecules,* 2025, **30**, DOI: 10.3390/molecules30153183.
31. Kama D.V., Frei A., Schutte-Smith M., Brink A., Swart C., Braband H., *et al.*, *New J. Chem.,* 2021, **45**, 22141-9, DOI: 10.1039/d1nj04273d.
32. Sousa L.S.d., Andrade A.L., Pinheiro A.d.A., Abreu F.D., Sousa E.H.S., Carvalho I.M.M.d., *et al.*, *Biofouling,* 2025, **41**, 1038-54.
33. Li F., Collins J.G., Keene F.R., *Chem. Soc. Rev.,* 2015, **44**, 2529-42, DOI: 10.1039/c4cs00343h.
34. Schindler K., Zobi F., *Molecules,* 2022, **27**, 539.
35. Lee L.C., Lo K.K., *J. Am. Chem. Soc.,* 2022, **144**, 14420-40, DOI: 10.1021/jacs.2c03437.
36. Hostachy S., Policar C., Delsuc N., *Coord. Chem. Rev.,* 2017, **351**, 172-88, DOI: 10.1016/j.ccr.2017.05.004.
37. Lee L.C., Leung K.K., Lo K.K., *Dalton Trans.,* 2017, **46**, 16357-80, DOI: 10.1039/c7dt03465b.
38. Guilbaud V., Kumar P., Grosjean A., Delfourne E., Boggio-Pasqua M., Mallet-Ladeira S., *et al.*, *Spectrochim. Acta A Mol. Biomol. Spectrosc.,* 2026, **344**, 126647, DOI: 10.1016/j.saa.2025.126647.
39. Le Garrec S., Martins-Bessa D., Wolff M., Delavaux-Nicot B., Mallet-Ladeira S., Serpentini C.L., *et al.*, *Dalton Trans.,* 2024, **53**, 16512-29, DOI: 10.1039/d4dt01907e.
40. Vanucci-Bacque C., Wolff M., Delavaux-Nicot B., Abdallah A.M., Mallet-Ladeira S., Serpentini C.L., *et al.*, *Dalton Trans.,* 2024, **53**, 11276-94, DOI: 10.1039/d4dt00922c.
41. Machura B., Kruszynski R., Jaworska M., Kłak J., Mroziński J., *Polyhedron,* 2006, **25**, 2537-49, DOI: 10.1016/j.poly.2006.02.021.
42. Braband H., Imstepf S., Felber M., Spingler B., Alberto R., *Inorg. Chem.,* 2010, **49**, 1283-5, DOI: 10.1021/ic902114p.
43. Das S., Chakravorty A., *Eur. J. Inorg. Chem.,* 2006, **2006**, 2285-91, DOI: 10.1002/ejic.200501102.
44. Schindler K., Cortat Y., Nedyalkova M., Crochet A., Lattuada M., Pavic A., *et al.*, *Pharmaceuticals,* 2022, **15**, 1107, DOI: 10.3390/ph15091107.
45. Nasiri Sovari S., Kolly I., Schindler K., Djuric A., Srdic-Rajic T., Crochet A., *et al.*, *Dalton Trans.,* 2023, **52**, 6934-44, DOI: 10.1039/d2dt04041g.
46. Cortat Y., Nedyalkova M., Schindler K., Kadakia P., Demirci G., Nasiri Sovari S., *et al.*, *Antibiotics,* 2023, **12**, 619, DOI: 10.3390/antibiotics12030619.
47. Mashaly M.M., El-Shafiy H.F., El-Maraghy S.B., Habib H.A., *Spectrochim. Acta A Mol. Biomol. Spectrosc.,* 2005, **61**, 1853-69, DOI: 10.1016/j.saa.2004.06.056.
48. Mashaly M.M., *J. Coord. Chem.,* 2010, **56**, 833-50, DOI: 10.1080/00958970310001140l1.

49. Maalaoui A., Said O.B., Akriche S.T., Al-Deyab S.S., Rzaigui M., *Z. Naturforsch. B,* 2012, **67**, 1178-84, DOI: 10.5560/znb.2012-0141.
50. Cooper S.M., Siakalli C., White A.J.P., Frei A., Miller P.W., Long N.J., *Dalton Trans.,* 2022, **51**, 12791-5, DOI: 10.1039/d2dt02157a.
51. Das S., Joshi P., Patra M., *Inorg. Chem.* 2023, **62**, 19720-33, DOI: 10.1021/acs.inorgchem.3c03110.
52. Vaidya S.P., M M., Chhatar S., Dey S., Patra C., Patra M., *Inorg. Chem. Front.,* 2023, **10**, 6711-27, DOI: 10.1039/d3qi01653f.
53. Mitsopoulou C.A., Dagas C., *Bioinorg. Chem. Appl.,* 2010, **2010**, 973742, DOI: 10.1155/2010/973742.
54. Logarto Parra A., Silva Yhebra R., Guerra Sardinas I., Iglesias Buela L., *Phytomedicine,* 2001, **8**, 395-400, DOI: 10.1078/0944-7113-00044.
55. Lewan L., Andersson M., Morales-Gomez P., *ALTA,* 1992, **20**, 297-301.
56. Mendes S.S., Marques J., Mesterhazy E., Straetener J., Arts M., Pissarro T.*, et al.*, *ACS Bio. Med. Chem. Au,* 2022, **2**, 419-36, DOI: 10.1021/acsbiomedchemau.2c00007.
57. Wenzel M., Patra M., Senges C.H., Ott I., Stepanek J.J., Pinto A.*, et al.*, *ACS Chem. Biol.,* 2013, **8**, 1442-50, DOI: 10.1021/cb4000844.
58. Novo D., Perlmutter N.G., Hunt R.H., Shapiro H.M., *Cytometry,* 1999, **35**, 55-63, DOI: 10.1002/(sici)1097-0320(19990101)35:1<55::Aid-cyto8>3.0.Co;2-2.
59. Van den Driessche F., Rigole P., Brackman G., Coenye T., *J. Microbiol. Methods,* 2014, **98**, 31-4.
60. Müller A., Wenzel M., Strahl H., Grein F., Saaki T.N., Kohl B.*, et al.*, *Proc. Natl. Acad. Sci.,* 2016, **113**, E7077-E86.
61. Boulos L., Prevost M., Barbeau B., Coallier J., Desjardins R., *J. Microbiol. Methods,* 1999, **37**, 77-86.
62. Kuru E., Hughes H.V., Brown P.J., Hall E., Tekkam S., Cava F.*, et al.*, *Angew. Chem. Int. Ed. Engl.,* 2012, **51**, 12519-23, DOI: 10.1002/anie.201206749.
63. Schindler B.D., Kaatz G.W., *Drug Resist. Updat.,* 2016, **27**, 1-13, DOI: 10.1016/j.drup.2016.04.003.
64. Lade H., Kim J.S., *Antibiotics,* 2023, **12**, 1362, DOI: 10.3390/antibiotics12091362.
65. Alexander J.A.N., Radaeva M., King D.T., Chambers H.F., Cherkasov A., Chatterjee S.S.*, et al.*, *J. Biol. Chem.,* 2020, **295**, 10870-84, DOI: 10.1074/jbc.RA120.013029.
66. Fishovitz J., Hermoso J.A., Chang M., Mobashery S., *IUBMB Life,* 2014, **66**, 572-7, DOI: 10.1002/iub.1289.
67. Alexander J.A.N., Worrall L.J., Hu J., Vuckovic M., Satishkumar N., Poon R.*, et al.*, *Nature,* 2023, **613**, 375-82, DOI: 10.1038/s41586-022-05583-3.
68. Lovering A.L., Gretes M.C., Safadi S.S., Danel F., de Castro L., Page M.G.*, et al.*, *J. Biol. Chem.,* 2012, **287**, 32096-102, DOI: 10.1074/jbc.M112.355644.
69. Valentin J.D.P., Straub H., Pietsch F., Lemare M., Ahrens C.H., Schreiber F.*, et al.*, *ISME J.,* 2022, **16**, 1176-86, DOI: 10.1038/s41396-021-01157-9.
70. Kuru E., Tekkam S., Hall E., Brun Y.V., Van Nieuwenhze M.S., *Nat. Protoc.,* 2015, **10**, 33-52, DOI: 10.1038/nprot.2014.197.
71. Shapley J.R., Inorganic Syntheses, **34**, John Wiley & Sons, 2004.
72. Nagaraj K., Senthil Murugan K., Thangamuniyandi P., Sakthinathan S., *J. Fluoresc.,* 2014, **24**, 1701-14, DOI: 10.1007/s10895-014-1457-1.
73. Wang C., Lystrom L., Yin H., Hetu M., Kilina S., McFarland S.A.*, et al.*, *Dalton Trans.,* 2016, **45**, 16366-78, DOI: 10.1039/c6dt02416e.

View Article Online
DOI: 10.1039/D6DT00824K

74. Machura B., Kruszynski R., *Polyhedron,* 2007, **26**, 3336-42, DOI: 10.1016/j.poly.2007.03.014.
75. National Committee for Clinical Laboratory Standards; Barry A.L., *CLSI,* 1999, **19**.
76. Wiegand I., Hilpert K., Hancock R.E., *Nat. Protoc.,* 2008, **3**, 163-75, DOI: 10.1038/nprot.2007.521.
77. Rahmani F., Demirci G., Cortat Y., Crochet A., Zobi F., *ChemBioChem,* 2025, **26**, e202401025.
78. Banti C.N., Hadjikakou S.K., *Bio-protoc.,* 2021, **11**, e3895-e.
79. Riss T., Moravec R., Niles A., Duellman S., Benink H., Worzella T.*, et al.*, *Cell Viability Assays, in Assay Guidance Manual*, ed. G. S. Sittampalam, N. P. Coussens, H. Nelson *et al.*, Eli Lilly & Company, 2004, https://www.ncbi.nlm.nih.gov/books/NBK144065/, (accessed 2026).
80. Frisch M.e., Trucks G., Schlegel H.B., Scuseria G., Robb M., Cheeseman J.*, et al.* Gaussian 16. Gaussian, inc. Wallingford, CT; 2016.
81. Adamo C., Barone V., *J. Chem. Phys.,* 1999, **110**, 6158-70.
82. Grimme S., Ehrlich S., Goerigk L., *J. Comput. Chem.,* 2011, **32**, 1456-65.
83. Weigend F., Ahlrichs R., *Phys. Chem. Chem. Phys.,* 2005, **7**, 3297-305.
84. Marenich A.V., Cramer C.J., Truhlar D.G., *J. Phys. Chem. B,* 2009, **113**, 6378-96.

View Article Online
DOI: 10.1039/D6DT00824K

Data availability

The data supporting this article have been included as part of the Electronic Supplementary Information (ESI). Crystallographic data for the compounds have been deposited at the Cambridge Crystallographic Data Centre (CCDC) under deposition numbers 2539772-2539777. Copies of the data can be obtained free of charge via the CCDC website. Additional data supporting the findings of this study are available from the corresponding author upon request.